A Novel Design of All-optical Full-adder Using Nonlinear X-shaped Photonic Crystal Resonators

Saleh Naghizade
Islamic Azad University Tabriz Branch
Hamed Saghaei (h.saghaei@iaushk.ac.ir)
Islamic Azad University Shahrekord Branch https://orcid.org/0000-0001-5588-3726

Research Article

Keywords: Full-adder, photonic crystal, optical Kerr effect, ring resonator

Posted Date: February 12th, 2021

DOI: https://doi.org/10.21203/rs.3.rs-215501/v1

Version of Record: A version of this preprint was published at Optical and Quantum Electronics on March 3rd, 2021. See the published version at https://doi.org/10.1007/s11082-021-02805-2.

Abstract

This paper proposes a new all-optical full-adder design based on nonlinear X-shaped photonic crystal (PhC) resonators. The PhC-based full-adder consists of three input ports, two X-shaped PhC resonators (X-PCRs), and two output ports. The dielectric rods made of silicon and nonlinear rods composed of doped glass are used to design the X-PCRs. Two well-known plane wave expansion and finite difference time domain methods are applied to study and analyze the photonic band structure and light propagation inside the PhC, respectively. Our numerical results demonstrate when the incoming light intensity increases, the nonlinear Kerr effect appears and manages the direction of light propagation inside the structure. The maximum time delay and footprint of the proposed full-adder are about 2.5ps and 663 $\mu m^{2,}$ making it an appropriate adder for high-speed data processing systems.

1. Introduction

High-speed processing is one of the excellent characteristics of photonics-based devices. Thus, professional optical systems require doing all the communication steps without using electrical signals in the optical domain. Signal processing is one of the important steps in optical systems and networks. All-optical logic devices are essential for realizing all-optical signal processing (Rahmani and Mehdizadeh 2018; Saghaei et al. 2017; Sharifi et al. 2016). One of the optical signal processes' high-tech devices is an optical full-adder because there exists a full-adder in every fundamental mathematical operator (Cheraghi et al. 2018; Jiang et al. 2015; Kowsari and Saghaei 2018; Liu and Ouyang 2008; Maleki et al. 2020; Sani et al. 2020; Vali-Nasab et al. 2019). A full-adder contains three input ports and two output ports; thus, three binary numbers are added together, and two binary numbers are obtained at the outputs called Sum and Carry. A photonic crystal (PhC) may have one or more photonic band gaps (PBGs) in particular wavelength ranges, which makes it capable of directing the light propagation inside a waveguide (Alipour-Banaei and Mehdizadeh 2013; Hosseinzadeh Sani et al. 2020a; Hosseinzadeh Sani et al. 2020b; Mehdizadeh et al. 2017b). PhCs ring resonators (PCRRs) provide excellent functionality to design and realize numerous optical devices with very small footprints and low fabrication cost. Therefore, they are more popular among researchers. Resonant modes of a PCRR depend on several key parameters such as rod radius, dielectric constant, and position of the PhC unit cells (Biswas et al. 2020; Farmani et al. 2020; Mansouri-Birjandi et al. 2016; Naghizade et al. 2018; Naghizade and Sattari-Esfahlan 2017; Tavousi et al. 2017). By changing every parameter, the blue or redshift occurs at resonant modes. Every PCRR has a resonant mode, acting as an optical pass-band or stop-band filter. So far, a large number of PhC-based devices such as optical filters (Alipour-Banaei et al. 2014; Foroughifar et al. 2021; Guo et al. 2019; Naghizade and Saghaei 2020a; Rakhshani and Mansouri-Birjandi 2013), logic gates (Andalib and Granpayeh 2009; Hussein et al. 2018; Parandin et al. 2018b; Younis et al. 2014), encoders and decoders (Moniem 2016; Naghizade and Khoshsima 2018; Parandin et al. 2018a), comparators (Fakouri-Farid and Andalib 2018; Jile 2020), adders and subtractors (Alipour-Banaei and Seif-Dargahi 2017; Hosseinzadeh Sani et al. 2020a; Karkhanehchi et al. 2017; Moradi 2019; Naghizade and Saghaei 2020b), registers (Martinez-Dorantes et al. 2017; Pahari and Guchhait 2012), and memories (Alexoudi et al. 2020;

Kuramochi et al. 2014; Uda et al. 2018), optical fibers (Aliee et al. 2020; Diouf et al. 2017; Ghanbari et al. 2018; Ghanbari et al. 2017; Saghaei 2017; Saghaei et al. 2016a; Saghaei et al. 2016b; Saghaei et al. 2015), demultiplexers (Mehdizadeh and Soroosh 2016; Saghaei et al. 2011; Saghaei and Seyfe 2008; Talebzadeh et al. 2017; Wen et al. 2012), sensors (Alden Mostaan and Saghaei 2021; Hosseinzadeh Sani et al. 2020b; Tabrizi et al. 2021; Tavakoli et al. 2019), PhC fibers (Ebnali-Heidari et al. 2014; Raei et al. 2018; Saghaei 2018; Saghaei and Ghanbari 2017; Saghaei and Van 2019), switches (Alipour-Banaei et al. 2015; Chen et al. 2006; Mehdizadeh et al. 2017a), interferometers (Gu et al. 2007; Saghaei et al. 2019), as well as all-optical clocked sequential circuits including flip-flops (Kumar et al. 2010; Sethi and Roy 2014), synchronous and asynchronous counters (Kaur and Kaler 2014; Poustie et al. 2000) have been designed and fabricated. New functionality is created using high nonlinear dielectric rods in the resonator, and switching applications can be achieved. Recently all-optical half-adders and full-adders were designed using linear and nonlinear effects, self-collimated beam, and coupled waveguides techniques in PhC structures (Ghadrdan and Mansouri-Birjandi 2013; Jiang et al. 2015; Neisy et al. 2018). In this paper, we present an all-optical full-adder using two X-shaped PCRRs. The plane wave expansion (PWE) and finite-difference time-domain (FDTD) methods are used to analyze the optical behavior of the proposed structure (Johnson and Joannopoulos 2001; Qiu 2002) The paper is organized as follows. The full-adder's physical structure and the numerical results achieved by the PWE method are presented in Sect. 2. Section 3 describes the light propagation inside the full-adder using the numerical FDTD method, and the paper is closed by the conclusion in Sect. 4.

2. Physical Structure

Figure 1 shows the schematic view of a typical full-adder and its truth table. We observe that a full-adder has been designed by combining two optical half-adders and an OR logic gate. Each half-adder consists of two input ports of A and B, and two output ports of S and C that S and C stand for Sum and Carry, respectively. The first half-adder output of S has been connected to the first input port of the second half-adder. C ports of optical half-adders are the OR gate's inputs and form the Carry of the final full adder and the S port of the second half-adder is also the Sum port of the full-adder. Besides, A, B, and C_{in} are the three input ports of the full-adder.

In this study, we aim to design an all-optical full-adder in a rod-based PhC. The fundamental PhC structure used to design the proposed structure consists of dielectric rods with hexagonal lattice geometry. The refractive index and radius of dielectric rods are assumed to be 3.46 and 0.2a, where a is the lattice constant of the PhC structure. Using the PWE method, the photonic band diagram of the fundamental structure has been calculated and shown in Fig. 2. It shows a wide PBG region at $0.27 < a/l < 0.45$ for TM polarization mode, which is equal to $1333\ \text{nm} < l < 2222\ \text{nm}$ for $a=600\ \text{nm}$. In addition to linear rods, an X-shaped PhC resonator (X-PCR) can be designed using several nonlinear dielectric rods in a specific location and direction. For this purpose, we have replaced a number of nonlinear rods with linear dielectric rods in X-PCR.

Nonlinear rods are made of doped glass whose linear refractive index and nonlinear Kerr coefficient are 1.4 and 10^{-14} m^2/W, respectively. Figure 3 demonstrates the X-PCR, where nonlinear rods are shown in dark green. As seen in the figure, the proposed resonator consists of one input port and three output ports.

An optical beam is launched in the bus waveguide and dropped to one of the nonlinear resonators' output ports depending on the input power. The time-domain light propagation inside X-PCR for two different optical powers are shown in Figs. 4(a), and 4(b). As shown in the figure, when the light power of $1W/\mu m^2$ enters the PhC structure, it exits the first output port (O_1) by creating a resonance mode in the X-PCR because the resonance mode is equal to the center wavelength of the input signal for this amount of optical power. When the optical power is $2W/\mu m^2$, resonance mode does not occur, and the optical beam continues to its direct path inside the bus waveguide and goes out from the second output port (O_2).

Figure 5 shows the proposed full-adder consisting of eight waveguides and two ring resonators at suitable places and directions inside the fundamental PhC structure. WG_1, WG_2, WG_3, and WG_4 waveguides and X-PCR_1 form the first half adder. The first half adder's S and C ports are placed at the right side of WG_3 and WG_4. Also, WG_4, WG_5, WG_6, and WG_7, and X-PCR_2 form the second half-adder. The right sides of WG_6 and WG_7 are the second half-adder C and S ports, respectively. WG_3, WG_6, and WG_8 form the OR gate and WG_8
works as the Carry port of the proposed full-adder. Also, the right side of the WG_7 works as the Sum output port, and A, B, and C are defined as the input ports of the full-adder. Both X-PCRs work with the same propagating method where the optical beam is coupled into the drop waveguide when the bus waveguide's optical power is $1W/\mu m^2$. However, it is not possible to couple light into other waveguides for optical power more than $1W/\mu m^2$.

3. Simulation Results

We employed the FDTD method to analyze and simulate the light propagation inside the proposed full-adder shown in Fig. 5, which contains three input ports. Therefore, according to the computation principle, we have 2^3 (2^N, N is the number of input ports) different input states. The optical power of the input ports is equal to $1W/mm^2$. The simulation results are discussed as follows for all states of the input ports.

Case #1: In this state, all the input ports are OFF (i.e., A=0, B=0, and C=0); thus, there is no optical signal in the structure, and both output ports are OFF, and the amounts of Sum and Carry will be zero.

Case #2: When A=1, B=0, and C=0, the optical signal coming from input port A, travels close to X-PCR_1 through WG_1 and WG_3. Since the optical power is less than $2W/mm^2$, the optical signal will be dropped into WG_4 using X-PCR_1 and propagates to WG_6. Again it is dropped into WG_7 using X-PCR_2 and travels toward Sum port. Thus, we have Sum=1 and Carry=0. The light propagation inside the proposed full-adder is shown in Fig. 6(a). Figure 6(b) shows that for this case, the normalized powers at Sum and Carry

output ports are more than 85% and less than 5%, respectively. Also, time delay; the time that output of proposed full-adder needs to achive a stable state is about 2.5 ps.

Case #3: When A=0, B=1, and C=0, the optical signal coming from input port B, travels close to X-PCR_1 through WG_2 and WG_3. Since the optical power is less than $2W/mm^2$, the optical signal will be dropped into WG_4 and propagates to WG_6, it is dropped into WG_7 using X-PCR_2 and travels toward the Sum output port, thus, we have Sum=1 and Carry=0. The light propagation inside the structure is shown in Fig. 7(a). Figure 7(b) shows that for this case, the normalized powers at Sum and Carry are more than 85% and less than 5%, respectively. Also, the time delay is about 2.5 ps.

Case #4: When A=0, B=0, and C=1, the optical signal coming from input port C, travels close to X-PCR_2 through WG_5 and WG_6. Since the optical power is less than $2W/mm^2$, the optical signal will be dropped into WG_7 and travels toward the Sum output port; thus, we have Sum=1 and Carry=0. The light propagation inside the structure is shown in Fig. 8(a). Figure 8(b) shows that for this case, the normalized powers at Sum and Carry are more than 90% and less than 1%, respectively. Also, time delay is about 2.5 ps.

Case #5: When A=1, B=1, and C=0, the optical signals coming from input ports A (in WG_1), and B (in WG_2) are combined at WG_3 and form a resultant signal with an optical power of $2W/mm^2$. Therefore, X-PCR_1 will not drop the optical beam from WG_3 into WG_4, and it travels toward Carry output port through WG_3 and WG_8. Indeed there is no optical beam inside WG_6 and Sum output port. Thus, in this case, Sum=0 and Carry=1. The light propagation inside the structure is shown in Fig. 9(a). Figure 9(b) shows that for this case, the normalized powers at Sum and Carry are more than 130% and less than 1%, respectively. Also, delay time is about 2.5 ps.

Case #6: When A=1, B=0, and C=1, the optical beam coming from input port A (in WG_1), travels close to X-PCR_1 through WG_3. Since the optical power is less than $2W/mm^2$, the optical signal will be dropped into WG_4. The optical beam coming from input port C propagates in WG_5 and is summed with the signal coming from WG_4 at the input of WG_6. Then the resultant signal is formed with an optical power of $2W/mm^2$. This new signal propagates inside WG_6. Since the optical power is $2W/mm^2$, the X-PCR_2 will not drop the optical beam from WG_6 into WG_7, and it travels toward Carry output port through WG_8. Thus, in this case, we will have Sum=0 and Carry=1. The light propagation inside the structure is shown in Fig. 10(a). Figure 10(b) shows that for this case, the normalized powers at Sum and Carry are less than 0.5% and more than 90%, respectively. Also, the delay is about 1.5 ps.

Case #7: When A=0, B=1, and C=1, the optical beam coming from input port B (in WG_2), propagates in the vicinity of the X-PCR_1 through WG_3. Since the optical power is less than $2W/mm^2$, the optical signal is dropped into WG_4. Similar to Case #6, the optical beam coming from input port C propagates inside WG_5 and is summed with the signal coming from WG_4 at the input of WG_6. Then the resultant signal is formed

with an optical power of 2W/mm^2 and propagates inside WG_6 and travels toward Carry output port through WG_8. Thus Sum=0 and Carry=1. The light propagation inside the structure is shown in Fig. 11(a). Figure 11(b) shows that for this case, the normalized powers at Sum and Carry are less than 0.5% and more than 90%, respectively. Also, the is about 1.5 ps.

Case #8: When A=1, B=1, and C=1, the optical signals coming from input ports A (in WG_1) and B (in WG_2) are combined at WG_3 and form a resultant signal with an optical power of 2W/mm^2. Therefore, X-PCR_1 does not drop the optical beam from WG_3 into WG_4, and it travels toward Carry output port through WG_3 and WG_8. The optical signal coming from input port C, travels close to X-PCR_2 through WG_5 and WG_6. Since the optical power is less than 2W/mm^2, the optical signal will be dropped into WG_7 and travels toward the Sum output port; thus, we have Sum=1 and Carry=1.

The light propagation inside the structure is shown in Fig. 12(a). Figure 12(b) shows that for this case, the normalized powers at Sum and Carry are more than 95% and 130%, respectively. Also, the time delay is about 2.5 ps. The output results of all eight input states are summarized in Table 1, and it shows that the proposed structure is acting as an all-optical full-adder.

Table 1: The outputs of the proposed full-adder for all eight input states.

Case	Input			Normalized Outputs (%)	
	A	B	C	Sum	Carry
#1	0	0	0	0	0
#2	1	0	0	85	0
#3	0	1	0	85	0
#4	0	0	1	90	0
#5	1	1	0	130	1
#6	1	0	1	0.5	90
#7	0	1	1	0.5	90
#8	1	1	1	95	130

4. Conclusion

In summary, we designed an all-optical full-adder based on nonlinear X-shaped PhC resonators in an area of 663 μm^2. The presented structure consisted of eight waveguides (by removing several silicon rods),

two nonlinear resonators, three input ports, and two output ports, all in a PhC microstructure composed of silicon rods in a hexagonal lattice. Eight different states for three input ports were simulated and discussed. The numerical results revealed that the proposed structure can be used as an all-optical full-adder with a maximum delay of about 2.5ps. Thus, it is an appropriate device for high-speed data processing in optical integrated circuits.

Declarations

Compliance with ethical standards

Conflict of interest: The authors declare that they have no known competing financial interests or personal relationships that could have appeared to influence the work reported in this paper.

References

1. Alden Mostaan, S.M., Saghaei, H.: A tunable broadband graphene-based metamaterial absorber in the far-infrared region. Opt. Quantum Electron. 53, 96 (2021). https://doi.org/10.1007/s11082-021-02744-y
2. Alexoudi, T., Kanellos, G.T., Pleros, N.: Optical RAM and integrated optical memories: a survey. Light Sci. Appl. 9, 1–16 (2020). https://doi.org/10.1038/s41377-020-0325-9
3. Aliee, M., Mozaffari, M.H., Saghaei, H.: Dispersion-flattened photonic quasicrystal optofluidic fiber for telecom C band operation. Photonics Nanostructures - Fundam. Appl. 40, 100797 (2020). https://doi.org/10.1016/j.photonics.2020.100797
4. Alipour-Banaei, H., Jahanara, M., Mehdizadeh, F.: T-shaped channel drop filter based on photonic crystal ring resonator. Optik (Stuttg). 125, 5348–5351 (2014)
5. Alipour-Banaei, H., Mehdizadeh, F.: Bandgap calculation of 2D hexagonal photonic crystal structures based on regression analysis. J. Opt. Commun. 34, 285–293 (2013)
6. Alipour-Banaei, H., Mehdizadeh, F., Serajmohammadi, S., Hassangholizadeh-Kashtiban, M.: A 2* 4 all optical decoder switch based on photonic crystal ring resonators. J. Mod. Opt. 62, 430–434 (2015)
7. Alipour-Banaei, H., Seif-Dargahi, H.: Photonic crystal based 1-bit full-adder optical circuit by using ring resonators in a nonlinear structure. Photonics Nanostructures-Fundamentals Appl. 24, 29–34 (2017)
8. Andalib, P., Granpayeh, N.: All-optical ultracompact photonic crystal AND gate based on nonlinear ring resonators. J. Opt. Soc. Am. B. 26, 10 (2009). https://doi.org/10.1364/josab.26.000010
9. Biswas, U., Rakshit, J.K., Bharti, G.K.: Design of photonic crystal microring resonator based all-optical refractive-index sensor for analyzing different milk constituents. Opt. Quantum Electron. 52, 19 (2020)
10. Chen, Z., Li, Z., Li, B.: A 2-to-4 decoder switch in SiGe/Si multimode inteference. Opt. Express. 14, 2671 (2006). https://doi.org/10.1364/oe.14.002671

11. Cheraghi, F., Soroosh, M., Akbarizadeh, G.: An ultra-compact all optical full adder based on nonlinear photonic crystal resonant cavities. Superlattices Microstruct. 113, 359–365 (2018). https://doi.org/10.1016/j.spmi.2017.11.017
12. Diouf, M., Salem, A. Ben, Cherif, R., Saghaei, H., Wague, A.: Super-flat coherent supercontinuum source in As_388Se_612 chalcogenide photonic crystal fiber with all-normal dispersion engineering at a very low input energy. Appl. Opt. 56, 163 (2017). https://doi.org/10.1364/ao.56.000163
13. Ebnali-Heidari, M., Saghaei, H., Koohi-Kamali, F., Naser Moghadasi, M., Moravvej-Farshi, M.K.: Proposal for Supercontinuum Generation by Optofluidic Infiltrated Photonic Crystal Fibers. IEEE J. Sel. Top. Quantum Electron. 20, (2014). https://doi.org/10.1109/JSTQE.2014.2307313
14. Fakouri-Farid, V., Andalib, A.: Design and simulation of an all optical photonic crystal-based comparator. Optik (Stuttg). 172, 241–248 (2018). https://doi.org/10.1016/j.ijleo.2018.06.153
15. Farmani, A., Soroosh, M., Mozaffari, M.H., Daghooghi, T.: Optical nanosensors for cancer and virus detections. In: Nanosensors for Smart Cities. pp. 419–432. Elsevier (2020)
16. Foroughifar, A., Saghaei, H., Veisi, E.: Design and analysis of a novel four-channel optical filter using ring resonators and line defects in photonic crystal microstructure. Opt. Quantum Electron. 53, 101 (2021)
17. Ghadrdan, M., Mansouri-Birjandi, M.A.: Concurrent implementation of all-optical half-adder and AND & XOR logic gates based on nonlinear photonic crystal. Opt. Quantum Electron. 45, 1027–1036 (2013). https://doi.org/10.1007/s11082-013-9713-1
18. Ghanbari, A., Kashaninia, A., Sadr, A., Saghaei, H.: Supercontinuum generation for optical coherence tomography using magnesium fluoride photonic crystal fiber. Optik (Stuttg). 140, 545–554 (2017). https://doi.org/10.1016/j.ijleo.2017.04.099
19. Ghanbari, A., Kashaninia, A., Sadr, A., Saghaei, H.: Supercontinuum generation with femtosecond optical pulse compression in silicon photonic crystal fibers at 2500 nm. Opt. Quantum Electron. 50, (2018). https://doi.org/10.1007/s11082-018-1651-5
20. Gu, L., Jiang, W., Chen, X., Wang, L., Chen, R.T.: High speed silicon photonic crystal waveguide modulator for low voltage operation. Appl. Phys. Lett. 90, 71105 (2007). https://doi.org/10.1063/1.2475580
21. Guo, Y., Zhang, S., Li, J., Li, S., Cheng, T.: A sensor-compatible polarization filter based on photonic crystal fiber with dual-open-ring channel by surface plasmon resonance. Optik (Stuttg). 193, 162868 (2019). https://doi.org/10.1016/j.ijleo.2019.05.074
22. Hosseinzadeh Sani, M., Ghanbari, A., Saghaei, H.: An ultra-narrowband all-optical filter based on the resonant cavities in rod-based photonic crystal microstructure. Opt. Quantum Electron. 52, 295 (2020)(a). https://doi.org/10.1007/s11082-020-02418-1
23. Hosseinzadeh Sani, M., Saghaei, H., Mehranpour, M.A., Asgariyan Tabrizi, A.: A novel all-optical sensor design based on a tunable resonant nanocavity in photonic crystal microstructure applicable in MEMS accelerometers. Photonic Sensors. (2020)(b). https://doi.org/10.1007/s13320-020-0607-0

24. Hussein, H.M.E., Ali, T.A., Rafat, N.H.: New designs of a complete set of Photonic Crystals logic gates. Opt. Commun. 411, 175–181 (2018). https://doi.org/10.1016/j.optcom.2017.11.043
25. Jiang, Y.C., Liu, S. Bin, Zhang, H.F., Kong, X.K.: Realization of all optical half-adder based on self-collimated beams by two-dimensional photonic crystals. Opt. Commun. 348, 90–94 (2015). https://doi.org/10.1016/j.optcom.2015.03.011
26. Jile, H.: Realization of an all-optical comparator using beam interference inside photonic crystal waveguides. Appl. Opt. 59, 3714 (2020). https://doi.org/10.1364/ao.385744
27. Johnson, S., Joannopoulos, J.: Block-iterative frequency-domain methods for Maxwell's equations in a planewave basis. Opt. Express. 8, 173 (2001). https://doi.org/10.1364/oe.8.000173
28. Karkhanehchi, M.M., Parandin, F., Zahedi, A.: Design of an all optical half-adder based on 2D photonic crystals. Photonic Netw. Commun. 33, 159–165 (2017). https://doi.org/10.1007/s11107-016-0629-0
29. Kaur, S., Kaler, R.S.: 5 GHz all-optical binary counter employing SOA-MZIs and an optical NOT gate. J. Opt. (United Kingdom). 16, 35201 (2014). https://doi.org/10.1088/2040-8978/16/3/035201
30. Kowsari, A., Saghaei, H.: Resonantly enhanced all-optical switching in microfibre Mach–Zehnder interferometers. Electron. Lett. 54, 229–231 (2018). https://doi.org/10.1049/el.2017.4056
31. Kumar, R., Huybrechts, K., Liu, L., Spuessens, T., Roelkens, G., Geluk, E.J., Vries, T. De, Regreny, P., Thourhout, D. Van, Baets, R., Morthier, G.: An ultra-small, low-power all-optical flip-flop memory on a silicon chip. Opt. InfoBase Conf. Pap. 4, 182–187 (2010). https://doi.org/10.1038/nphoton.2009.268
32. Kuramochi, E., Nozaki, K., Shinya, A., Takeda, K., Sato, T., Matsuo, S., Taniyama, H., Sumikura, H., Notomi, M.: Large-scale integration of wavelength-addressable all-optical memories on a photonic crystal chip. Nat. Photonics. 8, 474–481 (2014). https://doi.org/10.1038/nphoton.2014.93
33. Liu, Q., Ouyang, Z.B.: All-optical half adder based on cross structures in two-dimensional photonic crystals. Guangzi Xuebao/Acta Photonica Sin. 37, 46–50 (2008). https://doi.org/10.1364/oe.16.018992
34. Maleki, M.J., Mir, A., Soroosh, M.: Designing an ultra-fast all-optical full-adder based on nonlinear photonic crystal cavities. Opt. Quantum Electron. 52, 1–11 (2020)
35. Mansouri-Birjandi, M.A., Tavousi, A., Ghadrdan, M.: Full-optical tunable add/drop filter based on nonlinear photonic crystal ring resonators. Photonics Nanostructures - Fundam. Appl. 21, 44–51 (2016). https://doi.org/10.1016/j.photonics.2016.06.002
36. Martinez-Dorantes, M., Alt, W., Gallego, J., Ghosh, S., Ratschbacher, L., Völzke, Y., Meschede, D.: Fast Nondestructive Parallel Readout of Neutral Atom Registers in Optical Potentials. Phys. Rev. Lett. 119, 180503 (2017). https://doi.org/10.1103/PhysRevLett.119.180503
37. Mehdizadeh, F., Alipour-Banaei, H., Serajmohammadi, S.: Study the role of non-linear resonant cavities in photonic crystal-based decoder switches. J. Mod. Opt. 64, 1233–1239 (2017)(a). https://doi.org/10.1080/09500340.2016.1275854
38. Mehdizadeh, F., Soroosh, M.: A new proposal for eight-channel optical demultiplexer based on photonic crystal resonant cavities. Photonic Netw. Commun. 31, 65–70 (2016).

https://doi.org/10.1007/s11107-015-0531-1

39. Mehdizadeh, F., Soroosh, M., Alipour-Banaei, H., Farshidi, E.: A novel proposal for all optical analog-to-digital converter based on photonic crystal structures. IEEE Photonics J. 9, 1–11 (2017)(b). https://doi.org/10.1109/JPHOT.2017.2690362
40. Moniem, T.A.: All-optical digital 4 × 2 encoder based on 2D photonic crystal ring resonators. J. Mod. Opt. 63, 735–741 (2016). https://doi.org/10.1080/09500340.2015.1094580
41. Moradi, R.: All optical half subtractor using photonic crystal based nonlinear ring resonators. Opt. Quantum Electron. 51, 119 (2019). https://doi.org/10.1007/s11082-019-1831-y
42. Naghizade, S., Khoshsima, H.: Low input power an all optical 4×2 encoder based on triangular lattice shape photonic crystal. J. Opt. Commun. 1, 1–8 (2018). https://doi.org/10.1515/joc-2018-0019
43. Naghizade, S., Mohammadi, S., Khoshsima, H.: Design and simulation of an all optical 8 to 3 binary encoder based on optimized photonic crystal or gates. J. Opt. Commun. 410, 793–798 (2018). https://doi.org/10.1515/joc-2018-0034
44. Naghizade, S., Saghaei, H.: Tunable graphene-on-insulator band-stop filter at the mid-infrared region. Opt. Quantum Electron. 52, 224 (2020)(a). https://doi.org/10.1007/s11082-020-02350-4
45. Naghizade, S., Saghaei, H.: A Novel Design of All-Optical Half-Adder Using a Linear Defect in Photonic Crystal Microstructure. J. Appl. Res. Electr. Eng. (2020)(b)
46. Naghizade, S., Sattari-Esfahlan, S.M.: Loss-less elliptical channel drop filter for WDM applications. J. Opt. Commun. 40, 379–384 (2017). https://doi.org/10.1515/joc-2017-0088
47. Neisy, M., Soroosh, M., Ansari-Asl, K.: All optical half adder based on photonic crystal resonant cavities. Photonic Netw. Commun. 35, 245–250 (2018)
48. Pahari, N., Guchhait, A.: All-optical Serial Data Transfer between Registers using optical non-linear materials. Optik (Stuttg). 123, 462–466 (2012). https://doi.org/10.1016/j.ijleo.2011.05.006
49. Parandin, F., Karkhanehchi, M.M., Naseri, M., Zahedi, A.: Design of a high bitrate optical decoder based on photonic crystals. J. Comput. Electron. 17, 830–836 (2018)(a). https://doi.org/10.1007/s10825-018-1147-3
50. Parandin, F., Malmir, M.R., Naseri, M., Zahedi, A.: Reconfigurable all-optical NOT, XOR, and NOR logic gates based on two dimensional photonic crystals. Superlattices Microstruct. 113, 737–744 (2018)(b). https://doi.org/10.1016/j.spmi.2017.12.005
51. Poustie, A., Manning, R.J., Kelly, A.E., Blow, K.J.: All-optical binary counter. Opt. Express. 6, 69 (2000). https://doi.org/10.1364/oe.6.000069
52. Qiu, M.: Effective index method for heterostructure-slab-waveguide-based two-dimensional photonic crystals. Appl. Phys. Lett. 81, 1163–1165 (2002). https://doi.org/10.1063/1.1500774
53. Raei, R., Ebnali-Heidari, M., Saghaei, H.: Supercontinuum generation in organic liquid–liquid core-cladding photonic crystal fiber in visible and near-infrared regions: publisher's note. J. Opt. Soc. Am. B. 35, 1545 (2018). https://doi.org/10.1364/josab.35.001545

54. Rahmani, A., Mehdizadeh, F.: Application of nonlinear PhCRRs in realizing all optical half-adder. Opt. Quantum Electron. 50, 30 (2018). https://doi.org/10.1007/s11082-017-1301-3
55. Rakhshani, M.R., Mansouri-Birjandi, M.A.: Realization of tunable optical filter by photonic crystal ring resonators. Optik (Stuttg). 124, 5377–5380 (2013). https://doi.org/10.1016/j.ijleo.2013.03.114
56. Saghaei, H.: Supercontinuum source for dense wavelength division multiplexing in square photonic crystal fiber via fluidic infiltration approach. Radioengineering. 26, 16–22 (2017). https://doi.org/10.13164/re.2017.0016
57. Saghaei, H.: Dispersion-engineered microstructured optical fiber for mid-infrared supercontinuum generation. Appl. Opt. 57, 5591 (2018). https://doi.org/10.1364/ao.57.005591
58. Saghaei, H., Ebnali-Heidari, M., Moravvej-Farshi, M.K.: Midinfrared supercontinuum generation via As_2Se_3 chalcogenide photonic crystal fibers. Appl. Opt. 54, 2072 (2015). https://doi.org/10.1364/ao.54.002072
59. Saghaei, H., Elyasi, P., Karimzadeh, R.: Design, fabrication, and characterization of Mach–Zehnder interferometers. Photonics Nanostructures - Fundam. Appl. 37, 100733 (2019). https://doi.org/10.1016/j.photonics.2019.100733
60. Saghaei, H., Ghanbari, A.: White light generation using photonic crystal fiber with sub-micron circular lattice. J. Electr. Eng. 68, 282–289 (2017). https://doi.org/10.1515/jee-2017-0040
61. Saghaei, H., Heidari, V., Ebnali-Heidari, M., Yazdani, M.R.: A systematic study of linear and nonlinear properties of photonic crystal fibers. Optik (Stuttg). 127, 11938–11947 (2016)(a). https://doi.org/10.1016/j.ijleo.2016.09.111
62. Saghaei, H., Moravvej-Farshi, M.K., Ebnali-Heidari, M., Moghadasi, M.N.: Ultra-Wide Mid-Infrared Supercontinuum Generation in As40Se60 Chalcogenide Fibers: Solid Core PCF Versus SIF. IEEE J. Sel. Top. Quantum Electron. 22, (2016)(b). https://doi.org/10.1109/JSTQE.2015.2477048
63. Saghaei, H., Seyfe, B.: New approach to closed-loop power control in cellular CDMA systems under multipath fading. In: 2008 International Conference on Wireless Communications, Networking and Mobile Computing, WiCOM 2008 (2008)
64. Saghaei, H., Seyfe, B., Bakhshi, H., Bayat, R.: Novel approach to adjust the step size for closed-loop power control in wireless cellular code division multiple access systems under flat fading. IET Commun. 5, 1469–1483 (2011). https://doi.org/10.1049/iet-com.2010.0029
65. Saghaei, H., Van, V.: Broadband mid-infrared supercontinuum generation in dispersion-engineered silicon-on-insulator waveguide. J. Opt. Soc. Am. B. 36, A193 (2019). https://doi.org/10.1364/josab.36.00a193
66. Saghaei, H., Zahedi, A., Karimzadeh, R., Parandin, F.: Line defects on photonic crystals for the design of all-optical power splitters and digital logic gates. Superlattices Microstruct. 110, 133–138 (2017). https://doi.org/10.1016/j.spmi.2017.08.052
67. Sani, M.H., Tabrizi, A.A., Saghaei, H., Karimzadeh, R.: An ultrafast all-optical half adder using nonlinear ring resonators in photonic crystal microstructure. Opt. Quantum Electron. 52, 107 (2020). https://doi.org/10.1007/s11082-020-2233-x

68. Sethi, P., Roy, S.: Ultrafast All-Optical Flip-Flops, Simultaneous Comparator-Decoder and Reconfigurable Logic Unit with Silicon Microring Resonator Switches. IEEE J. Sel. Top. Quantum Electron. 20, 118–125 (2014). https://doi.org/10.1109/JSTQE.2013.2295179
69. Sharifi, H., Hamidi, S.M., Navi, K.: A new design procedure for all-optical photonic crystal logic gates and functions based on threshold logic. Opt. Commun. 370, 231–238 (2016)
70. Tabrizi, A.A., Saghaei, H., Mehranpour, M.A., Jahangiri, M.: Enhancement of absorption and effectiveness of a perovskite thin-film solar cell embedded with Gold nanospheres. Plasmonics. (2021). https://doi.org/10.1007/s11468-020-01341-1
71. Talebzadeh, R., Soroosh, M., Kavian, Y.S., Mehdizadeh, F.: Eight-channel all-optical demultiplexer based on photonic crystal resonant cavities. Optik (Stuttg). 140, 331–337 (2017). https://doi.org/10.1016/j.ijleo.2017.04.075
72. Tavakoli, F., Zarrabi, F.B., Saghaei, H.: Modeling and analysis of high-sensitivity refractive index sensors based on plasmonic absorbers with Fano response in the near-infrared spectral region. Appl. Opt. 58, (2019). https://doi.org/10.1364/AO.58.005404
73. Tavousi, A., Mansouri-Birjandi, M.A., Ghadrdan, M., Ranjbar-Torkamani, M.: Application of photonic crystal ring resonator nonlinear response for full-optical tunable add–drop filtering. Photonic Netw. Commun. 34, 131–139 (2017)
74. Uda, T., Ishii, A., Kato, Y.K.: Single Carbon Nanotubes as Ultrasmall All-Optical Memories. ACS Photonics. 5, 559–565 (2018). https://doi.org/10.1021/acsphotonics.7b01104
75. Vali-Nasab, A.M., Mir, A., Talebzadeh, R.: Design and simulation of an all optical full-adder based on photonic crystals. Opt. Quantum Electron. 51, (2019). https://doi.org/10.1007/s11082-019-1881-1
76. Wen, K., Yan, L., Pan, W., Luo, B., Guo, Z., Guo, Y.: Wavelength demultiplexing structure based on a plasmonic metal-insulator-metal waveguide. J. Opt. (United Kingdom). 14, 75001 (2012). https://doi.org/10.1088/2040-8978/14/7/075001
77. Younis, R.M., Areed, N.F.F., Obayya, S.S.A.: Fully integrated and and or optical logic gates. IEEE Photonics Technol. Lett. 26, 1900–1903 (2014). https://doi.org/10.1109/LPT.2014.2340435

Figures

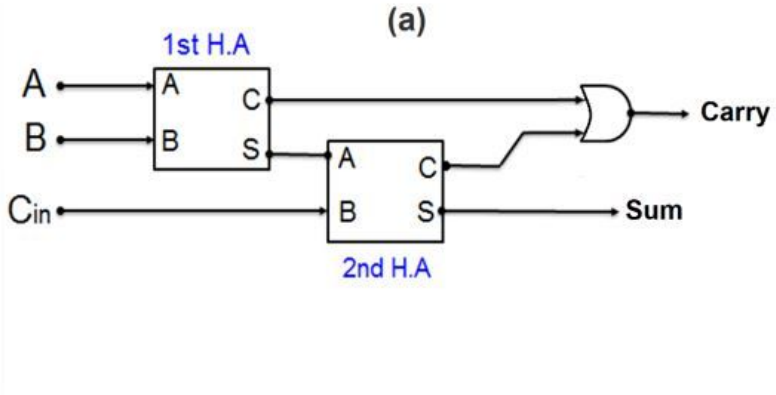

(b)

Input			Output	
A	B	Cin	Sum	Carry
0	0	0	0	0
0	0	1	1	0
0	1	0	1	0
0	1	1	0	1
1	0	0	1	0
1	0	1	0	1
1	1	0	0	1
1	1	1	1	1

Figure 1

Illustration of (a) the full-adder circuit consisting of two half-adders and an OR logic gate, three input ports of A, B, and Cin, and two output ports of Sum and Carry, (b) the truth table of full-adder for all states.

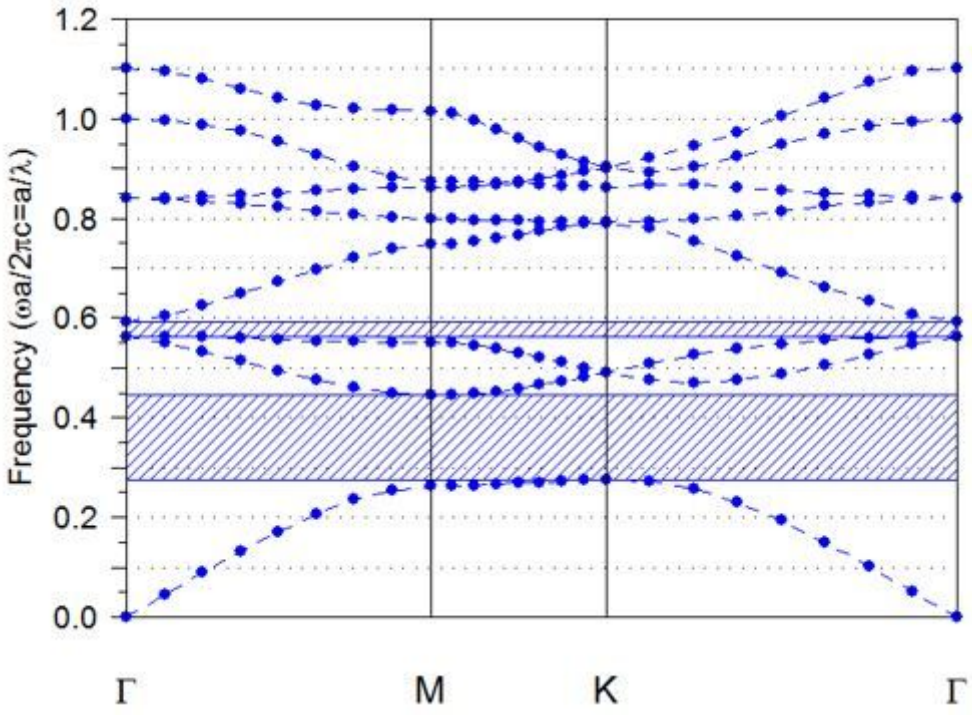

Figure 2

Photonic band diagram of the fundamental rod-based PhC for the TM polarization mode.

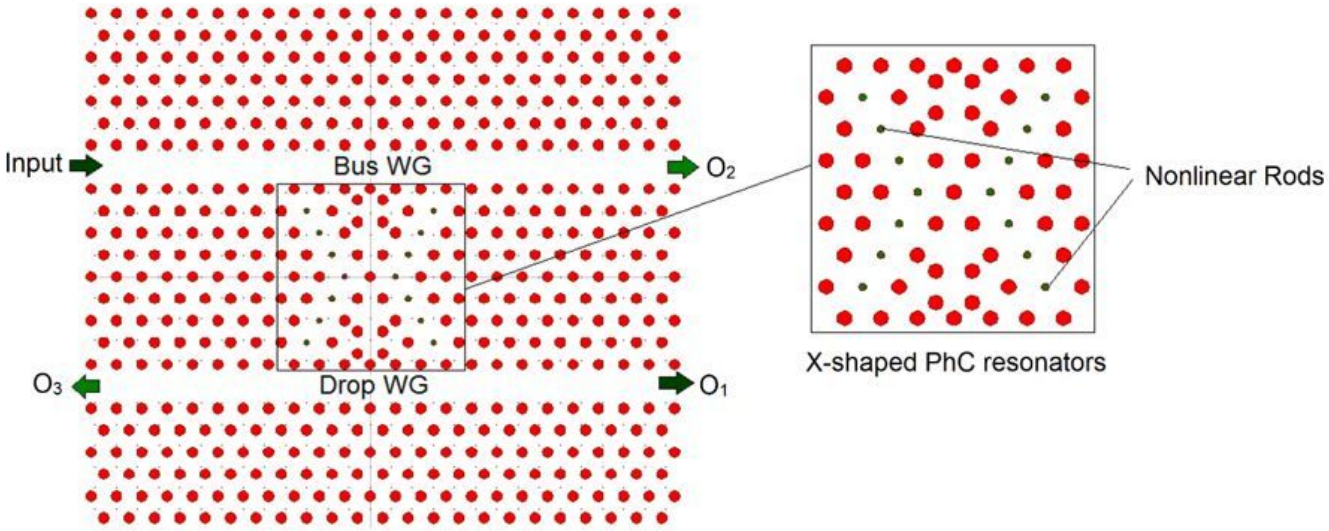

Figure 3

The schematic view of X-shaped PhC resonator composed of linear and nonlinear rods.

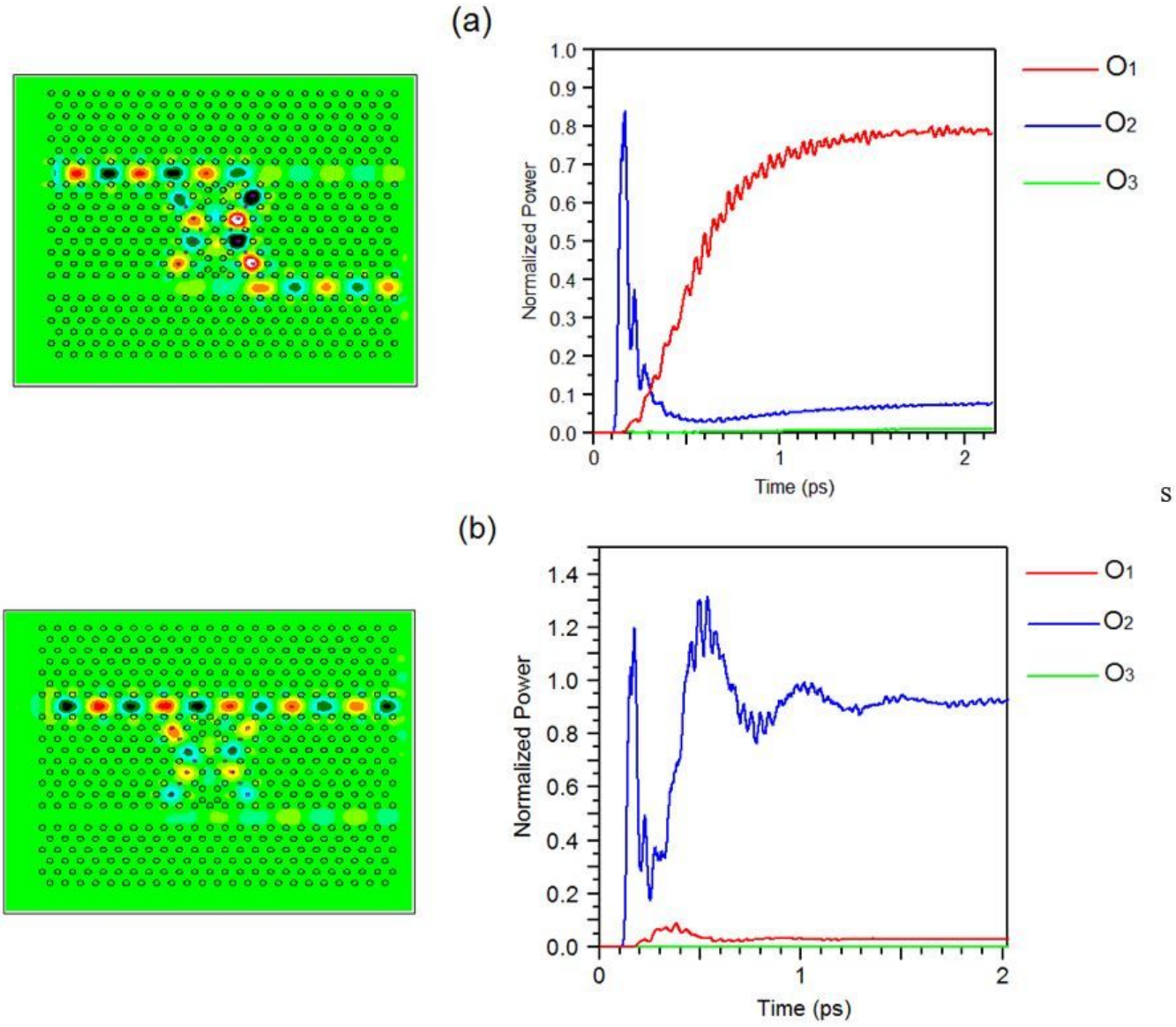

Figure 4

Light propagation inside the X-PCR for different input powers of (a) P=1W/μm2 and (b) P=2W/μm2.

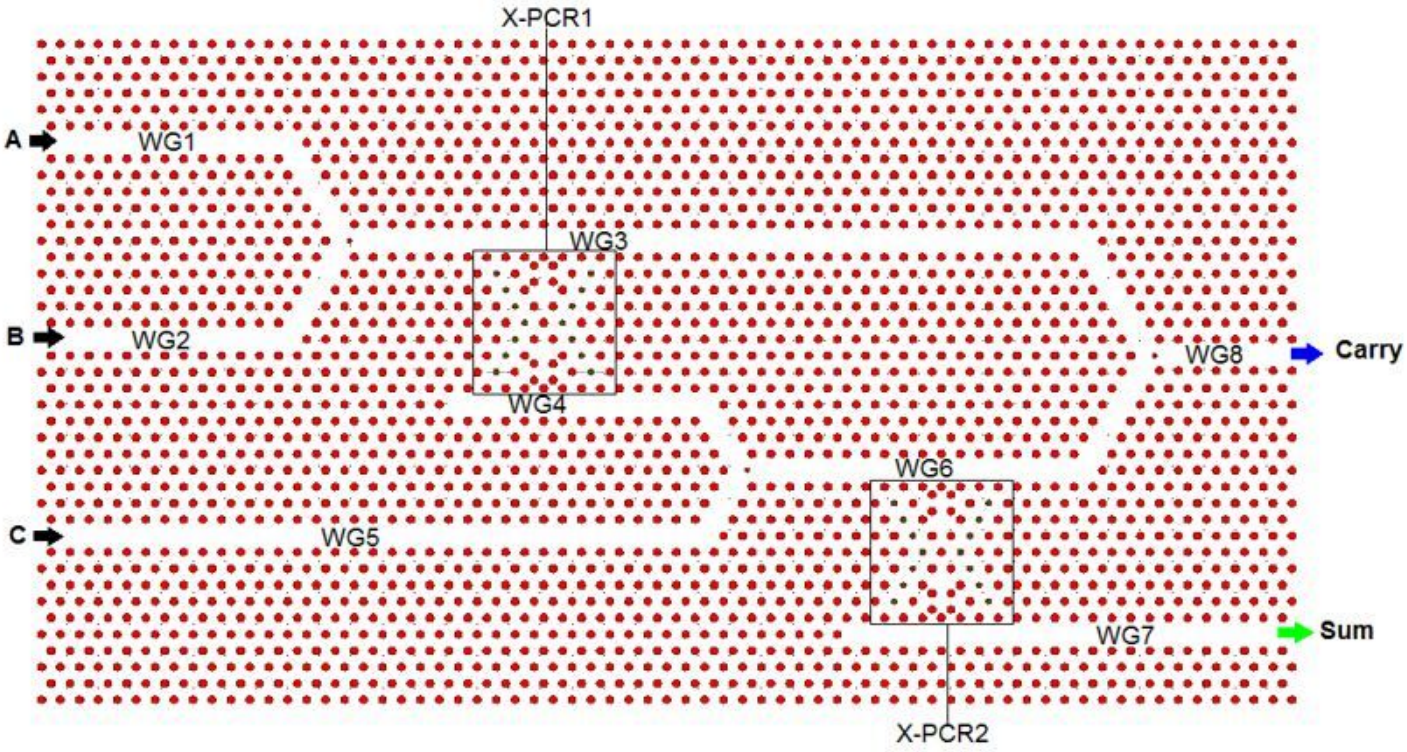

Figure 5

The proposed all-optical full-adder consisting of eight waveguides and two ring resonators.

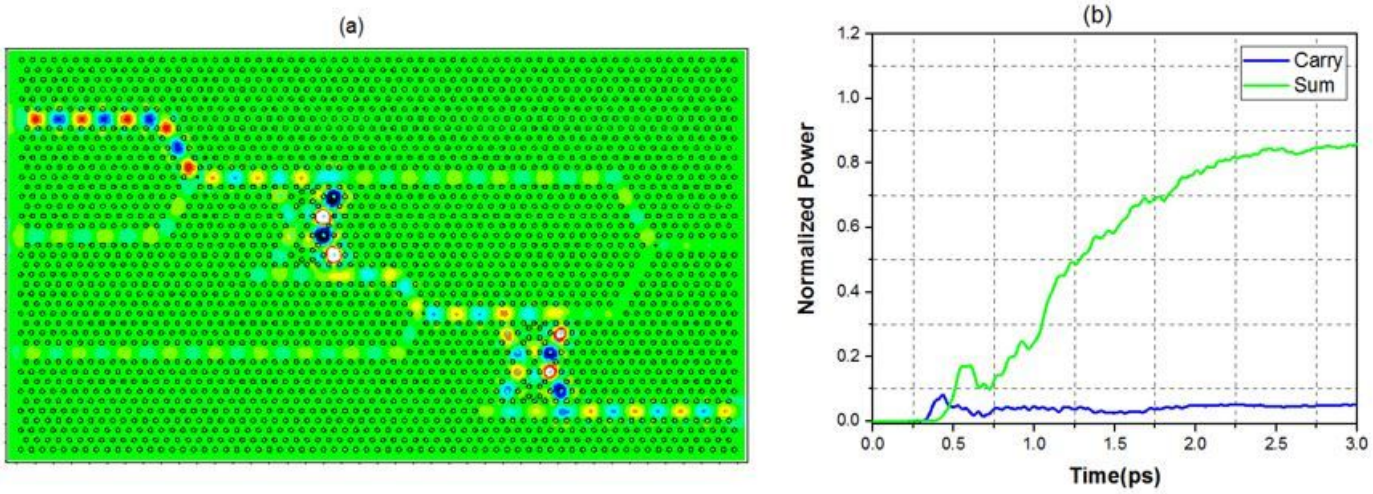

Figure 6

Illustration of (a) light propagation and (b) output powers of the proposed full-adder for Case #2.

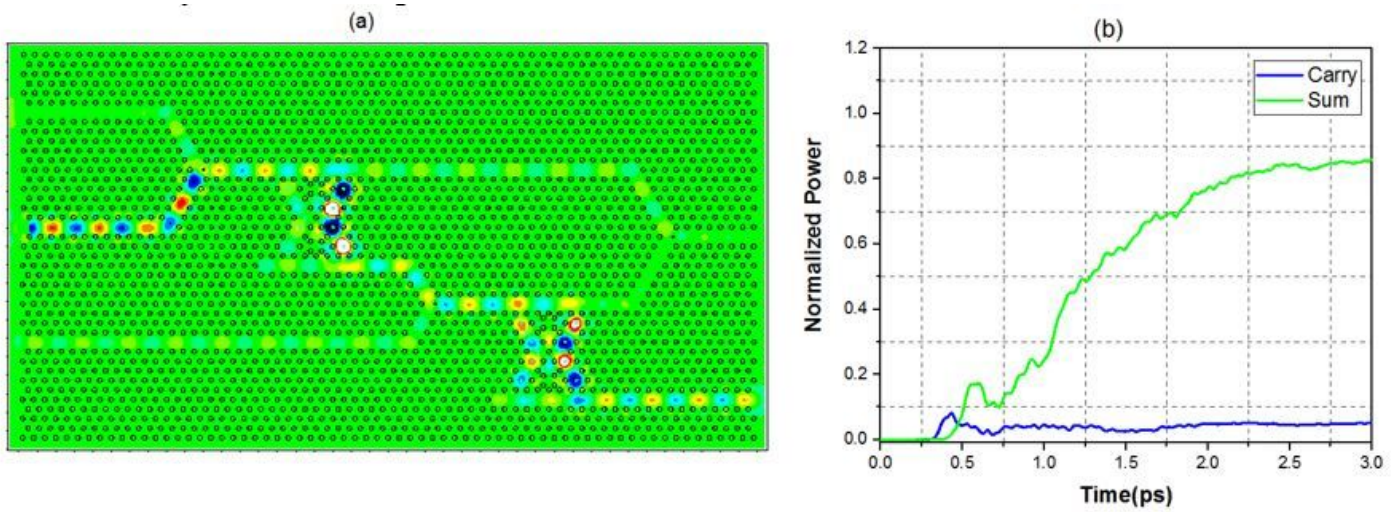

Figure 7

Illustration of (a) light propagation and (b) output powers of the proposed full-adder for Case #3.

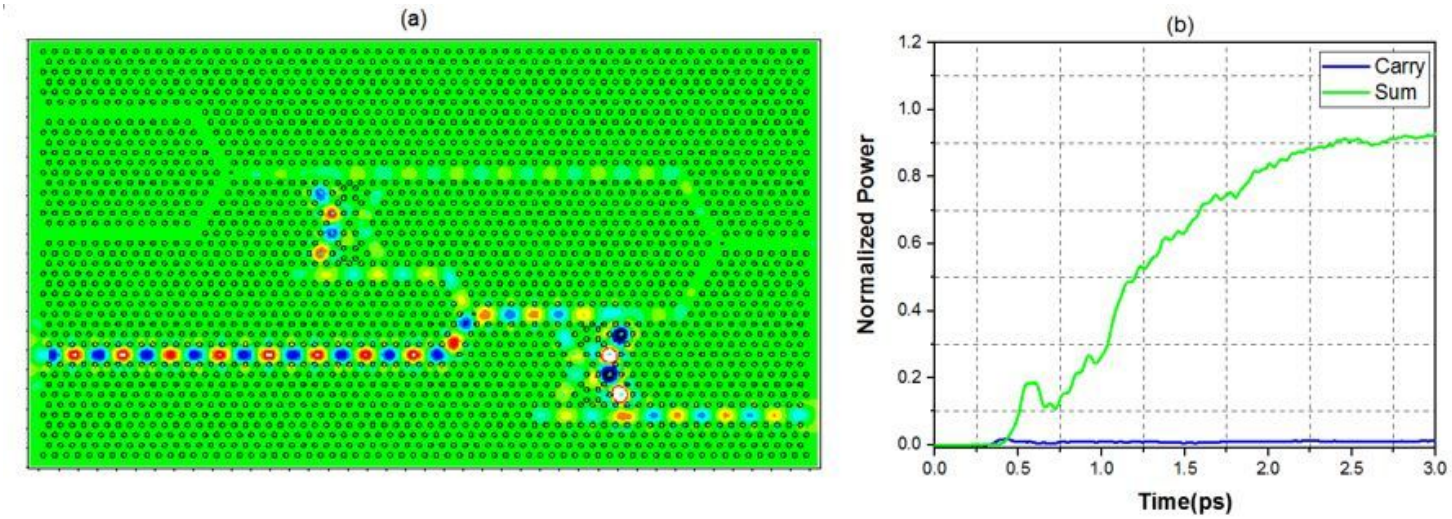

Figure 8

Illustration of (a) light propagation and (b) output powers of the proposed full-adder for Case #4.

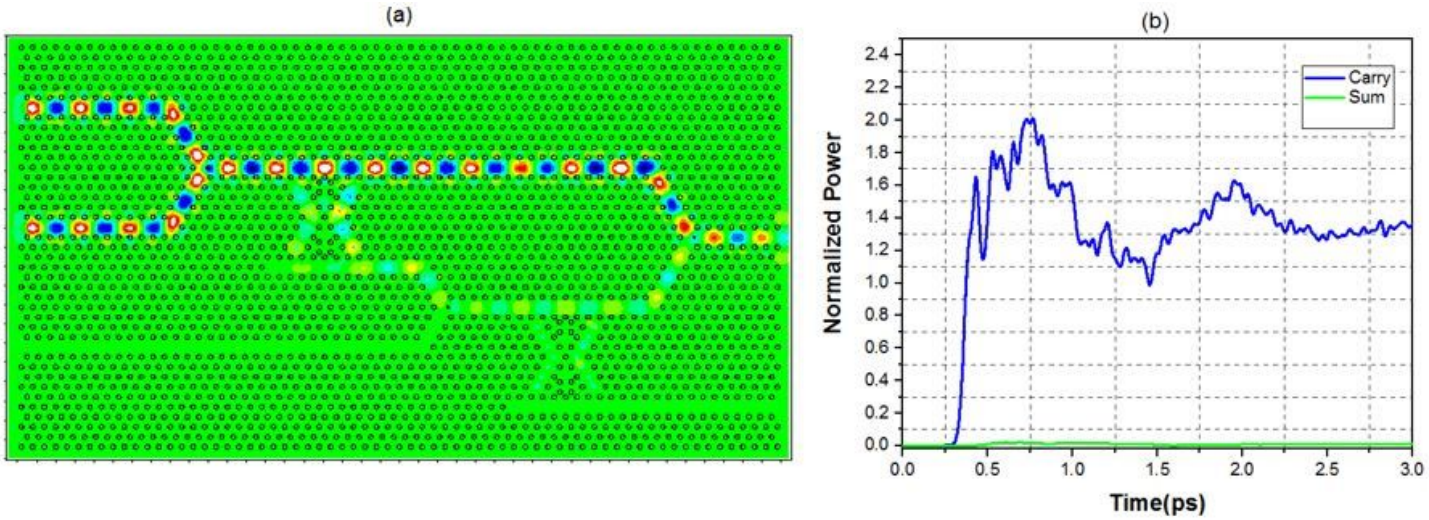

Figure 9

Illustration of (a) light propagation and (b) output powers of the proposed full-adder for Case #5.

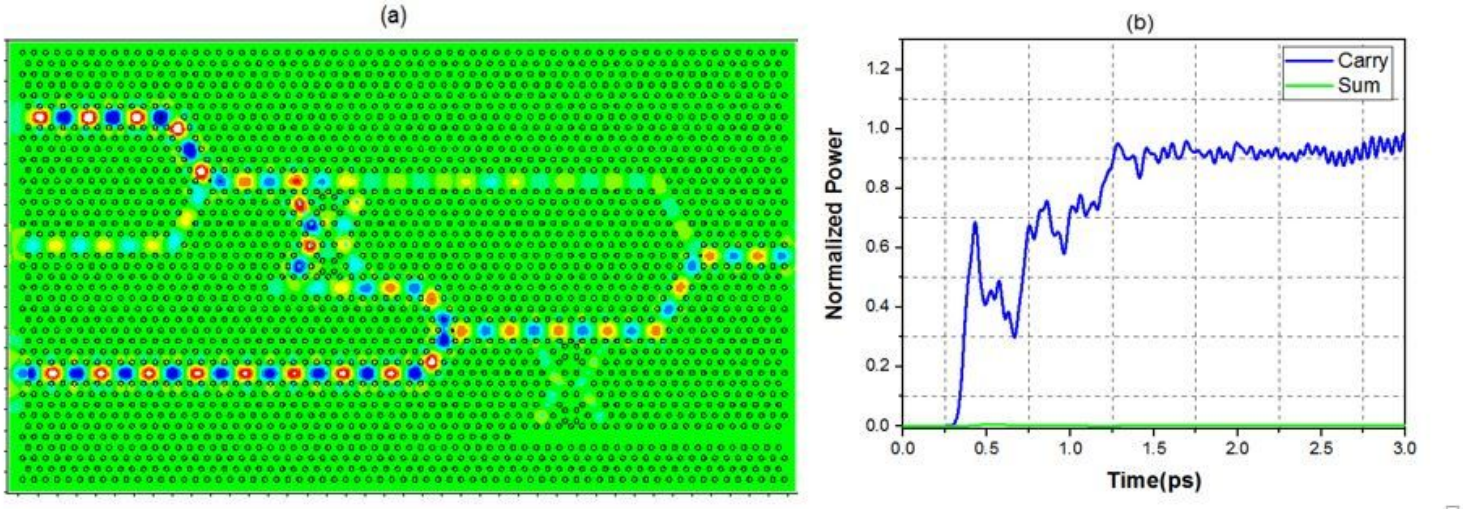

Figure 10

Illustration of (a) light propagation and (b) output powers of the proposed full-adder for Case #6.

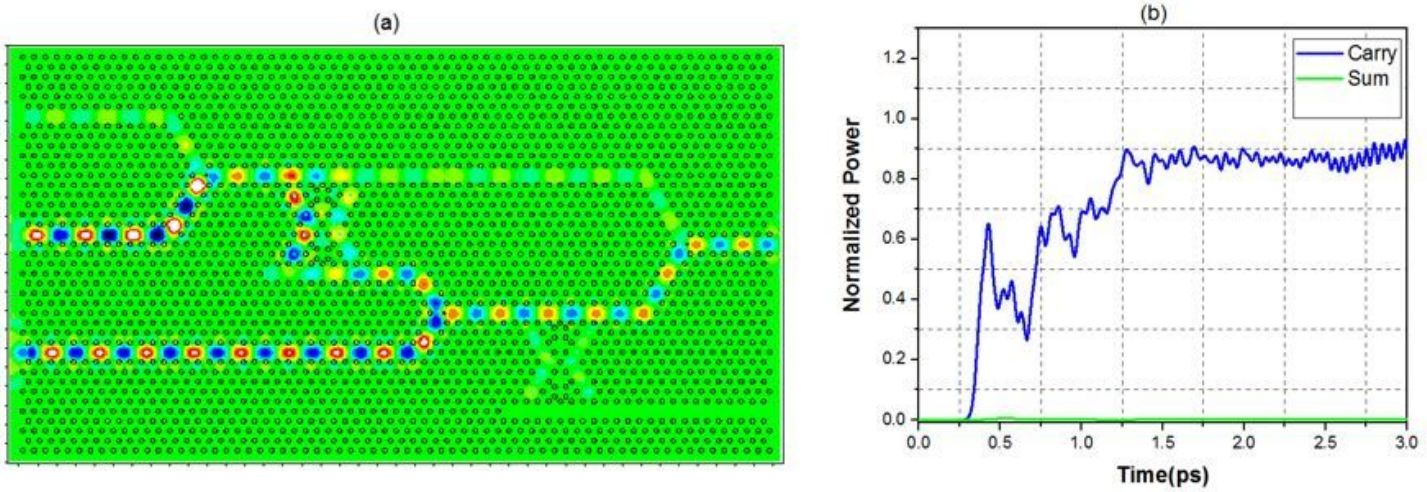

Figure 11

Illustration of (a) light propagation and (b) output powers of the proposed full-adder for Case #7.

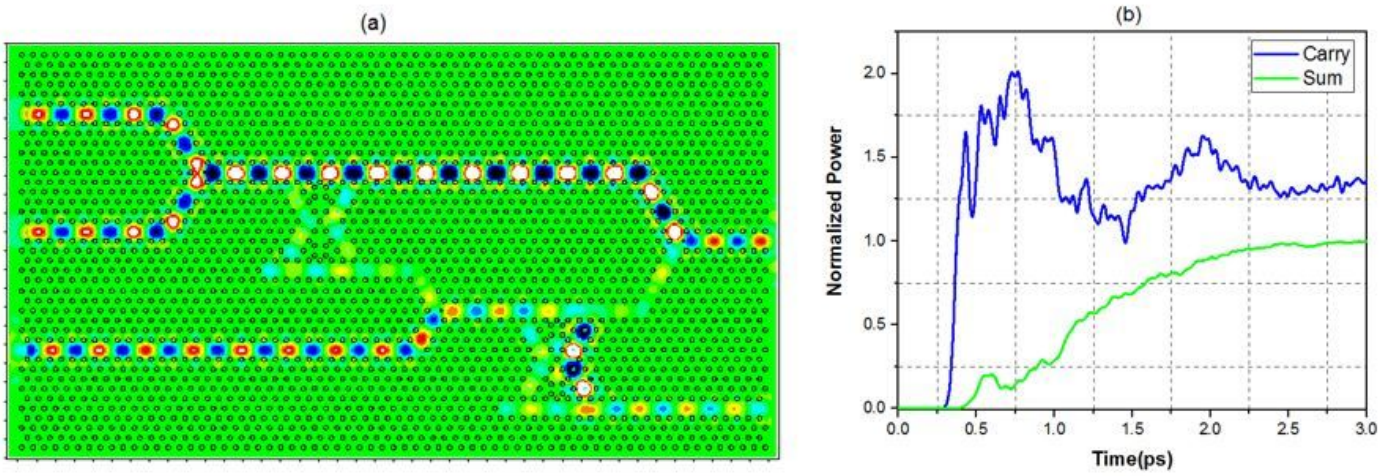

Figure 12

Illustration of (a) light propagation and (b) output powers of the proposed full-adder for Case #8.